QUANTITATIVE CHARACTERISATION OF MOLLUSC SHELL TEXTURES

D. CHATEIGNER
Laboratoire de Physique de l'Etat Condensé, Université Du Maine, Le Mans, France
C. HEDEGAARD
Institute of Biology, Department of Ecology and Genetics, University of Aarhus, Denmark
H.-R. WENK
Department of Geology and Geophysics, University of California, Berkeley, USA

Abstract

Textures of monoplacophora, cephalopod, bivalve and gastropod mollusc shells, composed of aragonite and calcite, vary in strength and pattern. The study emphasises textures of nacre and preferred orientation of aragonite but for some species calcite layers were analysed. Texture strength varies from random to extremely high. The aragonite texture patterns commonly have **c** axes at high angles to the shell surface. The **a** axes exhibit various patterns, from an ideal fibre texture to a perfect single crystal-like orientation, with or without presence of {110} twinning. Large texture differences are found between shells from phyllogenetically distant families, whereas textures of closely related species are more similar. A compact textural terminology is introduced to describe the various texture patterns, and to facilitate comparison between species.

Keywords: mollusc, shell, nacre, biomimetics, aragonite, calcite

1 Introduction

The formation of calcium carbonates in natural processes such as mollusc shells is of increasing interest (Urist 1965), particularly due to biomimetic relationships. For example, it has been shown that nacre from *Pinctada maxima* could be incorporated in sheep bones and stimulate bone generation by human osteoblasts (Lopez & al. 1992). Therefore a quantification of the internal microstructure and texture of shells are important. Also, since shells are the only preserved parts in fossils, their texture can become a classification criterion for paleontologists. Also, a non-trivial relationship between the crystallographic textures and shell microstructures, as seen with SEM, was revealed (Hedegaard et Wenk, 1998). Textures differ in shell structures with similar morphological patterns between distantly related molluscs, and may vary between layers within an individual (Chateigner et al. 1996). This work quantifies texture

differences in shells from gastropods, bivalves, cephalopods, and monoplacophora. Wishing to explore the extent of the phylogenetic signal in textures, we undertook a systematic survey of many samples. We found it practical to use a compact notation based on the actual observations and a systematic nomenclature which helps to compare the species.

2 Samples, texture experiments

Shell specimens were provided by the University of California Museum of Paleontology, Berkeley, the Laboratoire de Biologie Animale, Le Mans and our own collections. A detailed description of the microstructural arrangements (nacre, crossed lamellar ...) can be found in Hedegaard (1990). We selected sample pairs of closely related taxa. The x-ray measurements and data corrections were detailed elsewhere (Chateigner et al., 1996). The quantitative texture analysis was done using the Berkeley Texture Package (Wenk et al. 1998). When a good reproducibility of the experimental pole figures and satisfying reliability factors were obtained, the OD was used to recalculate the {001} and {100} pole figures. Typical results for reliability are presented in a previous work (Chateigner et al. 1996). For all these experiments, the growth direction, **G**, perpendicular to the margin of the shell at the beam location is the vertical axis of our pole figures. The plane tangent to the shell at the beam location, defined by the sample holder plane, has its normal, **N**, as the normal axes of the pole figures. The third axis, **M**, direction of the growth lines is then horizontal on the pole figures. Unless specifically indicated all discussions refer to the orthorhombic mineral aragonite that composes most mollusc nacre.

3 c axis distributions

We are describing in this paragraph the orientations of the **c** axis component of the layers (aragonite or calcite) relative to **N**, by an angle α that makes the maximum of the distribution with **N**. A quite common feature, $\mathbf{c}_{\perp}$, corresponds to α=0, like for the inner sheet nacre layer (ISN) of *Pinctada maxima* (Fig. 1a). Some species exhibit deviations from this orientation. In the inner comarginal crossed lamellar (ICCL) layer of *Nerita polita*, **c** axes are inclined towards **G** by α=15° (Fig. 1b).

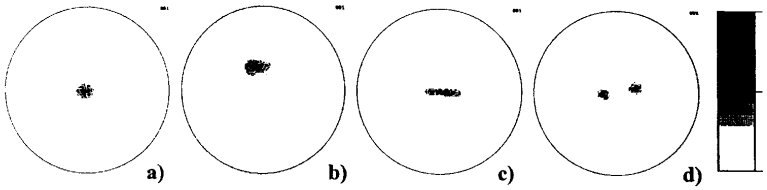

Fig. 1: recalculated {001} pole figures of *Pinctada maxima* (maximum density > 100 m.r.d.) **(a)**, *Nerita polita* (max: 29 m.r.d.) **(b)**, *Fragum fragum* (max: 35 m.r.d.) **(c)** and *Cypraea testudinaria* (max > 100 m.r.d.) **(d)**. Linear density scale, equal area projection. Minimum densities are 0.

The ICCL layer of *Fragum fragum* shows a wide dispersion of the **c** axes in a plane around **G**, with a FWHM of α=15 (Fig. 1c). The ICCL layer of *Cypraea testudinaria*

exhibits a splitting of the **c** axes into two components from **N**, at α=30° from each other (Fig. 1d).

4 a axis distribution and twinning

Many **a** axis patterns are observed. The outer comarginal crossed lamellar layer (OCCL) of *Helix pomatia* (Fig. 2a) shows a single crystal-like pattern, with **a** axes located at β=90° from **G**. The inner columnar nacre layer (ICN) of *Tectus niloticus* (Fig. 2b) shows a <001> fibre texture. In the case of tilted or split **c** axes, β refers to the crystalline direction located in the tangent plane (usually **a**, **b** or <110>). Between the perfect fibre and the single crystal **a** axis distributions, intermediate patterns are observed, larger distributions like in the ISN layer of *Lampsilis alatus* (not shown here) or twinning. In the context of this paper "twinning" simply means twinning-like patterns because with the methods used in this study we can not identify actual twin intergrowths. Due to the pseudosymmetry of the aragonite structure (Bragg, 1937), crystallites can share one of their (110) crystallographic planes, causing twinning. This results in domains where the **a** axes are separated by an angle close to 60°, where successive domains can rearrange in hexagonal shaped platelets like in nacre. Such hexagonal domains can then be either at random or preferably oriented to one another. On {100} pole figures, twinning in aragonite gives rise to 4 or 6 poles, 4 if one twin system ((110) or $(1\,\bar{1}\,0)$) is activated, 6 if both are, here referred to as single and double twinning, respectively. For instance, single twinning is observed in the ICCL layer of *Conus leopardus* (Fig. 2c), and double twinning in the ICN layer of *Nautilus pompilius* (Fig. 2d). We can evaluate the percentage of twinned volume from texture component intensities, V_x and V_* respectively for single and double twinning, from the ratio between the {100} poles corresponding to the twinning, and all the twin components. The calculation gives V_* = 61% of twinned volume for *Nautilus pompilius* (close to the maximum of 67% for this twinning type) and V_x = 46% for *Cypraea mus* (close to the maximum of 50%).

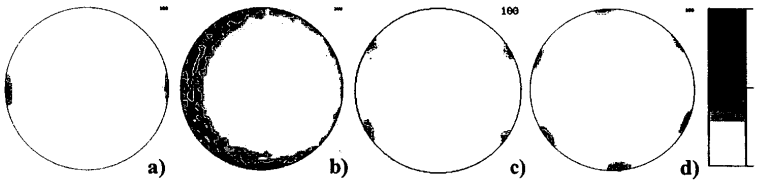

Fig. 2: recalculated {100} pole figures of *Helix pomatia* (max: 55 m.r.d.) **(a)**, *Tectus niloticus* (max: 8 m.r.d.) **(b)**, *Conus leopardus* (max: 49 m.r.d.) **(c)** and *Nautilus pompilius* (max: 23 m.r.d.) **(d)**. Linear density scale, equal area projection. Minimum densities are 0.

In twinned patterns, β refers to the most intense component of the {100} poles or to the closest to **G**.

5 Textural nomenclature and discussion

A description of the microstructure (crossed lamellar, nacre) including all the important texture characteristics is necessary, particularly if several layers are present in each species. A compact description may be useful for an efficient comparison between samples. We propose, for a particular layer, L, in the shell, to specify the **c** and **a** axes dispersions, and quantify the presence of twinning and splitting. These terms may be included in $\langle c, \alpha | \mathbf{L} | P_T^{a,\beta} \rangle$ where L depends on the location in the shell (inner, outer, comarginal) and on its microstructure. The left hand side of the bracket describes the **c** axes pattern, $\perp$ for $\mathbf{c}_\perp$, $\angle$ for one tilted component, $\vee$ for a split and $\forall$ for a dispersion. The right hand side describes the **a** axes pattern. P is ● for no texture, ⊙ stands for a fibre texture, × for a single twin, * for a double twin and | for the absence of twin. T is the percentage of twinned volume. β and α were defined previously. Using this textural description, the OCCL layer of *Helix pomatia* is described by the 'texture term' $\langle \perp | O | I^{a,90} \rangle$, while the ICCL layer of *Cypraea testudinaria* and the ISN layer of *Pinctada maxima* are $\langle \vee,15 | ICCL | I^{a} \rangle$ and $\langle \perp | ISN | *_{14}^{a,90} \rangle$ respectively. Fig. 3 is a proposal for a phylogenetic tree, that includes texture results. For this work we mainly focus our discussion on the nacre inner layers and on the variation of the texture strength through the thickness, for some shells. First of all, we observe many significant deviations from the usually assumed growth relationships, with <100> and <001> respectively aligned with **G** and **N**. The **a** axes are often found at 90° from **G**, for instance in the *HELIX* or *EUGLANDINA* species. Inclined, tilt and dispersed **c** axes are observed in both bivalves and gastropods, but not in Nautiloidea, nor in Monoplacophora, though theses two latter families are only represented by four analysed species. The gastropods family exhibits the largest variability of texture patterns, from fibres to single-crystal like orientations. The inner nacre layers only show $\mathbf{c}_\perp$ axes except for *Haliotis cracherodi*. In bivalves, the *Neotrigonia*, *Pteria* and *Pinctada* analysed species have ISN layers with $\mathbf{c}_\perp$ axes and around 10% of double twinning, while other analysed branches exhibit more varied texture patterns and larger twinning ratios. For ICCL layers, 50% of single twinning occurs (except for *Paphia solanderi*) with split **c**-axes, and <110> are aligned with **G**. In gastropods, the ICN layers are <001> fibre textures, as for monoplacophoras, while ICCL or ICoCL (complex crossed lamellar) layers exhibit variable **c** and **a** axes patterns. Looking at texture variations with thickness from the interior towards the outside of the shell, we find that the outsides are generally less organised than the internal layers. For instance in the gastropod *Conus leopardus*, the ICCL layer is single twinned (with a texture index of 201 m.r.d.^{2} and an entropy S=-5.16), while the outer radial crossed lamellar (ORCL) layer is a fibre (F^2=29 m.r.d.^{2} and S=-2.65). This is also true for the bivalve *Paphia solanderi* for which both the ICCL and outer simple prismatic (OSiP) layers are fibre textures (ICCL: F^2=177 m.r.d.^{2} and S=-5.06; OSiP: F^2=44 m.r.d.^{2} and S=-3.28). Consequently it appears that fibre textures are mainly located on the outside of the shells. This feature appears to be independent of the crystalline phase, e.g. for *Viana regina*. In this species, a progressive loss of the fibre texture strength is observed, from the ICCL layer (S=-3.22), to the OCCL (S=-1.78), to the outside homogeneous calcitic (OHC) layer (S=-0.55).

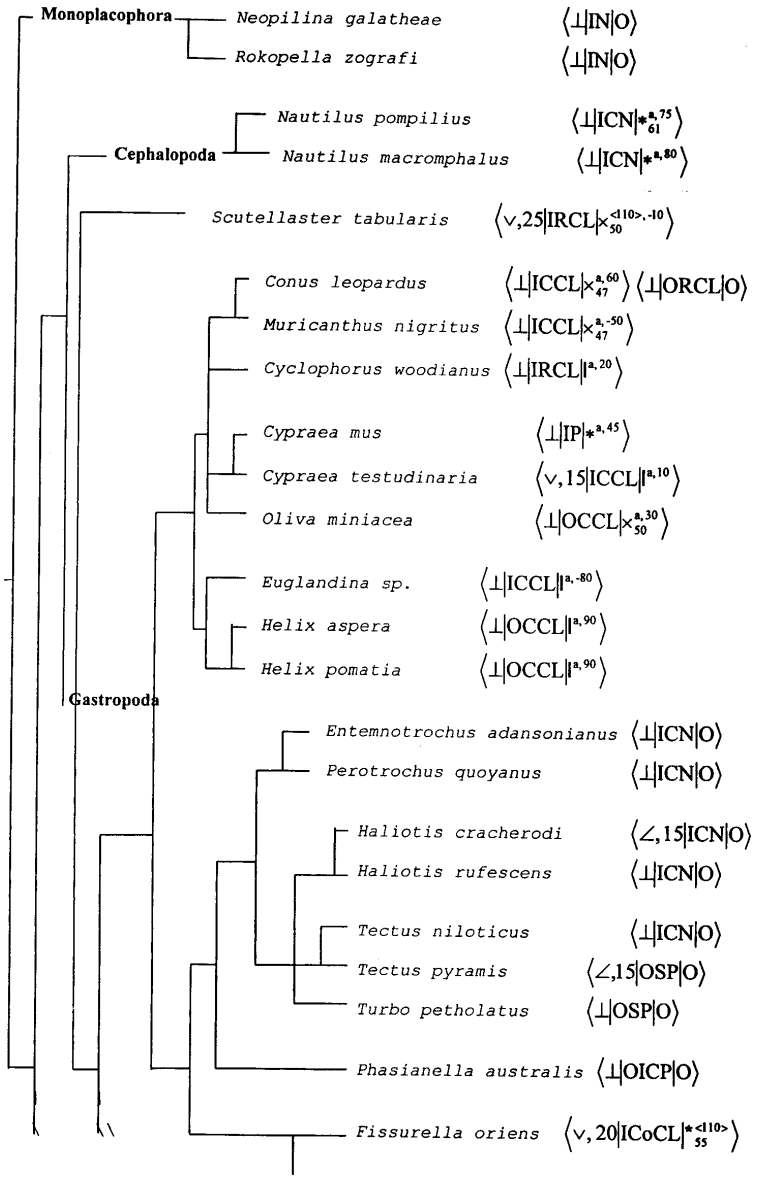
Monoplacophora
Neopilina galatheae ⟨⊥|IN|O⟩
Rokopella zografi ⟨⊥|IN|O⟩
Cephalopoda
Nautilus pompilius ⟨⊥|ICN|*a,75 61⟩
Nautilus macromphalus ⟨⊥|ICN|*a,80⟩
Scutellaster tabularis ⟨v,25|IRCL|×<110>,-10 50⟩
Gastropoda
Conus leopardus ⟨⊥|ICCL|×a,60 47⟩ ⟨⊥|ORCL|O⟩
Muricanthus nigritus ⟨⊥|ICCL|×a,-50 47⟩
Cyclophorus woodianus ⟨⊥|IRCL|Ia,20⟩
Cypraea mus ⟨⊥|IP|*a,45⟩
Cypraea testudinaria ⟨v,15|ICCL|Ia,10⟩
Oliva miniacea ⟨⊥|OCCL|×a,30 50⟩
Euglandina sp. ⟨⊥|ICCL|Ia,-80⟩
Helix aspera ⟨⊥|OCCL|Ia,90⟩
Helix pomatia ⟨⊥|OCCL|Ia,90⟩
Entemnotrochus adansonianus ⟨⊥|ICN|O⟩
Perotrochus quoyanus ⟨⊥|ICN|O⟩
Haliotis cracherodi ⟨∠,15|ICN|O⟩
Haliotis rufescens ⟨⊥|ICN|O⟩
Tectus niloticus ⟨⊥|ICN|O⟩
Tectus pyramis ⟨∠,15|OSP|O⟩
Turbo petholatus ⟨⊥|OSP|O⟩
Phasianella australis ⟨⊥|OICP|O⟩
Fissurella oriens ⟨v,20|ICoCL|*<110> 55⟩

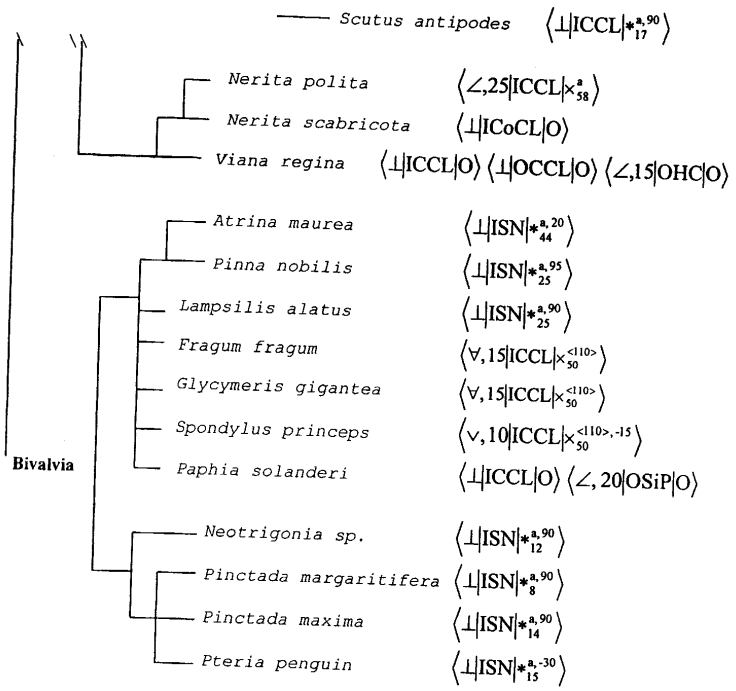

Fig. 3: Proposal for a phylogenetic tree, including textural patterns

These preliminary observations suggest that textural features are related to mollusc phylogeny. Pattern variations between branches are consistent are consistent with the actual mollusc phylogeny. Also, the loss of textural order or strength through the thickness of the shells is characterised by the texture entropy.

6 References

Bragg, W.-L. (1937). *Atomic Structures of Minerals*, Cornell Univ. Press, pp 114-126.

Chateigner, D., Hedegaard, C. and Wenk, H.-R. (1996). In Z. Liang, L. Zuo & Y. Chu *Textures of Materials*, vol. 2, pp 1221-1226.

Hedegaard, C. (1990). Thesis, University of Aarhus, Denmark, vol. 1 & 2.

Hedegaard, C. and Wenk, H.R. (1998). *J. Molluscan Studies*, 64, pp 133-136.

Lopez, E. & Vidal, B., Berland, S., Camprasse, S., Camprasse, G. and Silve, C. (1992), *Tissue & Cell*, 24(5), pp 667-679.

Urist M.-R. (1965), *Science*, 150, pp 893.

Wenk, H.-R., Matthies, S., Donovan, J. and Chateigner, D. (1998). *J. Appl. Cryst.* 31, pp 262-269.